NeuroImage: Clinical 36 (2022) 103242

Contents lists available at ScienceDirect

NeuroImage: Clinical

journal homepage: www.elsevier.com/locate/ynicl

# Radiomics for prediction of intracerebral hemorrhage outcomes: A retrospective multicenter study

Xiaoyu Huang [a,b,c,d,1], Dan Wang [a,1], Qiaoying Zhang [e], Yaqiong Ma [b,f], Hui Zhao [a,b,c,d], Shenglin Li [a,b,c,d], Juan Deng [a,b,c,d], Jialiang Ren [g], Jingjing Yang [a,b,c,d], Zhiyong Zhao [f], Min Xu [a,b,c,d], Qing Zhou [a,b,c,d], Junlin Zhou [a,c,d,h,*]

[a] Department of Radiology, Lanzhou University Second Hospital, Lanzhou 730030, China
[b] Second Clinical School, Lanzhou University, Lanzhou 730030, China
[c] Key Laboratory of Medical Imaging of Gansu Province, Lanzhou 730030, China
[d] Gansu International Scientific and Technological Cooperation Base of Medical Imaging Artificial Intelligence, Lanzhou 730030, China
[e] Department of Radiology, Xi'an Central Hospital, Xi An 710000, China
[f] Department of Radiology, Gansu Provincial Hospital, Lanzhou 730030, China
[g] GE Healthcare, Beijing 100176, China
[h] Department of Neurosurgery, Lanzhou University Second Hospital Lanzhou 730030, China

ARTICLE INFO

*Keywords:*
Intracerebral hemorrhage
Radiomics
Non-contrast computed tomography
Perihematomal edema
Outcome

ABSTRACT

*Background:* Accurate risk stratification of patients with intracerebral hemorrhage (ICH) could help refine adjuvant therapy selection and better understand the clinical course. We aimed to evaluate the value of radiomics features from hematomal and perihematomal edema areas for prognosis prediction and to develop a model combining clinical and radiomic features for accurate outcome prediction of patients with ICH.

*Methods:* This multicenter study enrolled patients with ICH from January 2016 to November 2021. Their outcomes at 3 months were recorded based on the modified Rankin Scale (good, 0–3; poor, 4–6). Independent clinical and radiomic risk factors for poor outcome were identified through multivariate logistic regression analysis, and predictive models were developed. Model performance and clinical utility were evaluated in both internal and external cohorts.

*Results:* Among the 1098 ICH patients evaluated (mean age, 60 ± 13 years), 703 (64 %) had poor outcomes. Age, hemorrhage volume and location, and Glasgow Coma Scale (GCS) were independently associated with outcomes. The area under the receiver operating characteristic curve (AUC) of the clinical model was 0.881 in the external validation cohort. Addition of the Rad-score (combined hematoma and perihematomal edema area) improved predictive accuracy and model performance (AUC, 0.893), net reclassification improvement, 0.140 ($P < 0.001$), and integrated discrimination improvement, 0.050 ($P < 0.001$).

*Conclusions:* The radiomics features of hematomal and perihematomal edema area have additional value in prognostic prediction; moreover, addition of radiomic features significantly improves model accuracy.

## 1. Introduction

Stroke is a major cause of death globally ("The top 10 causes of death," n.d.) and the leading cause of disability-adjusted life years (GBD 2016 Neurology Collaborators, 2019). Spontaneous intracerebral hemorrhage (ICH) is the second most common stroke subtype; however, there is no effective treatment for ICH (Andersen et al., 2009; Ironside et al., 2019). Early markers and accurate risk estimation of poststroke outcomes may help direct management, refine selection of adjuvant therapy, and improve patient prognosis recovery (Skajaa et al., 2022).

*Abbreviations:* ICH, intracerebral hemorrhage; PHE, perihematomal edema; NCCT, non-contrast computed tomography; mRS, modified Rankin Scale; GCS, Glasgow Coma Scale; AUC, area under the receiver operating characteristic curve; ROC, receiver operating characteristic; IDI, integrated discrimination improvement; NRI, net reclassification improvement.

* Corresponding author at: Department of Radiology, Lanzhou University Second Hospital, Lanzhou 730030, China.
*E-mail address:* ery_zhoujl@lzu.edu.cn (J. Zhou).

[1] Xiaoyu Huang and Dan Wang contributed equally to this work.

https://doi.org/10.1016/j.nicl.2022.103242
Received 25 August 2022; Received in revised form 15 October 2022; Accepted 18 October 2022
Available online 19 October 2022

Non-contrast computed tomography (NCCT) is the preferred examination modality for patients with ICH (Greenberg et al., 2022). Several imaging markers based on NCCT can predict hemorrhage expansion or poor outcomes; these radiological signs describe lesion characteristics and include the island sign (Li et al., 2017), the blend sign (Li et al., 2015), the black hole sign (Li et al., 2018), the hypodensity (Boulouis et al., 2016), and the hematoma maturity score (Serrano et al., 2022), among others.

However, although these signs can help radiologists determine lesion features, they are not quantitative and can result in inconsistencies due to subjectivity (Pszczolkowski et al., 2021). Moreover, although the I2 score, derived from dual-energy CT images based on CT angiography, may be a higher sensitivity marker (Tan et al., 2019), it is not routinely or properly performed during the diagnostic workup of acute ICH (Morotti et al., 2020). In contrast, NCCT-based imaging radiomics, a more objective and reproducible quantitative indicator, can result in higher accuracy. Recently, radiomics features have been associated with prognosis, even though they have restricted predictive performance for 3-month functional outcomes (Haider et al., 2021; Pszczolkowski et al., 2021; Song et al., 2021). Specifically, although radiomics models could predict functional outcome, their accuracy and stability need to be improved to be used clinically as reliable tools for predicting poor functional outcomes in ICH. Further, radiomic analyses of perihematomal edema (PHE) and effective outcome prediction are rare. PHE is the main cause of secondary brain injury post-ICH (Babi and James, 2017; Sprügel et al., 2019), and a possible therapeutic target for cerebral hemorrhage; however, its impact on ICH patient outcomes remains unclear (Wu et al., 2017; Yang et al., 2015). Furthermore, hematoma and PHE are usually analyzed separately, and the prognostic power of the radiomics features of PHE has yet to be elucidated. In addition, it is unclear whether and how hematoma and PHE data can improve the prognostic accuracy for ICH.

Thus, this study investigated whether a combination of hematoma and/or PHE radiomics features with clinical quantitative features based on early-stage NCCT could improve the accuracy and stability of prognostic prediction. Moreover, we investigated the mechanism by which the combination of hematoma and/or PHE radiomic features provides additional information on 3-month functional outcomes of ICH. Thus, we compared the predictive performance of different models after addition of radiomic features. Finally, the model with the best comprehensive performance was visualized.

## 2. Methods

### 2.1. Study design and sample

This retrospective study was reviewed and approved by the three centers involved. The requirement for informed consent was waived because of the retrospective nature of the study. All applicable data protection regulations were followed to ensure patient confidentiality.

The study was conducted in three tertiary teaching hospitals in China and included patients with spontaneous ICH who underwent brain NCCT between January 2016 and November 2021. The inclusion criteria were inpatients, age >18 years, undergoing NCCT for suspicion of ICH within 6 h after symptom onset, and ICH diagnosis. The exclusion criteria were craniotomy or hematoma evacuation before CT, acquired/secondary brain hemorrhage, tumor, trauma, cerebral aneurysm or infection, no PHE, and inadequate or problematic image quality. Finally, 1098 patients were included (Fig. S1). Patients from center 1 (Gansu, China), were divided into the training cohort (brain scan between Jan 2016 and Dec 2019, n = 814 patients) and the internal validation cohort (brain scan between Jan 2020 and Dec 2020, n = 198 patients). In addition, 86 patients who underwent brain scans between June 2021 and Nov 2021 from centers 2 (Gansu, China) and 3 (Shanxi, China) were included in the independent external validation cohort.

Data, including age, sex, Glasgow Coma Scale (GCS), and time from symptom onset to baseline CT, were obtained from medical records. Laboratory data at the timepoint closest to ICH ictus were also collected, including glucose, triglycerides, white blood cell, neutrophil, lymphocyte, and international normalized ratio. The 3-month functional outcomes were independently assessed by a senior neurologist through in-person interviews (Z.Y.Z 15 years of experience) or a phone call by trained study staff (X.Y.H., 6 years of experience), using the modified Rankin Scale (mRS) score. For patients lost to follow-up (13 cases), we used the functional status at discharge (Ferro et al., 2004). Unfavorable functional outcomes were defined as a dichotomized mRS score of 4–6 for poor outcome and 0–3 as good outcome (Shoamanesh et al., 2018).

### 2.2. Image acquisition and analysis

Baseline NCCT brain scans of the skull base to the cranium were acquired as part of routine clinical care. Only axial scans were accepted, and there were no restrictions on scanner manufacturer, scanner settings, or slice thickness (slice thickness: 1–5 mm; 120 KV, 148–440 mA). Digital Imaging and Communications in Medicine data were collected. Three neuroradiologists blinded to patient data and outcomes (S.L.L, J.D. with 3, and H.Z with 5 years of clinical experience in neuroradiology, respectively.) independently recorded the hematoma location (deep or lobar) (Pasi et al., 2021) and presence of other imaging signs, including intraventricular or subarachnoid hemorrhage, hypodensity, and midline shift. To improve interobserver consistency, only hypodensity signs were recorded. Any heterogeneous type within the hematoma was defined as positive “hypodensity sign” (Barras et al., 2009; Boulouis et al., 2016). The midline shift threshold was set to >4 mm (Yang et al., 2018).

### 2.3. Radiomics feature extraction and processing

First, the volume of interest (VOI) of the whole hematoma and PHE were manually segmented by three authors (S.L.L., J.D., and H.Z.) on the axial images according to the visible gross hematoma and PHE volume on ITK-SNAP software (http://www.itksnap.org, version 3.8.0). The final VOI was derived from the overlapping segmentation made by the three authors. If differences among the three VOIs >20 %, the VOI was redefined by author D.W., who has 6 years of diagnostic experience in neuroradiology in an academic full-service hospital (Su et al., 2020). The VOI volumes were recorded, and VOIs <125 $mm^3$ were excluded (Kniep et al., 2019) (Fig. S2).

Second, the radiomic analysis workflow is described in Fig. 1. Image normalization and radiomic feature extraction from VOIs were performed using the Artificial Intelligence Kit (A.K.) software version 3.2.2 (GE Healthcare, China). The feature extraction process followed the image biomarker standardization initiative guidelines (Zwanenburg et al., 2020b) (Supplementary Material). A total of 214 NCCT radiomics-based features, including 107 edema areas and 107 hematoma areas from seven categories (shape, first-order, gray level co-occurrence matrix [GLCM], gray-level run-length matrix [GLRLM], gray-level size zone matrix [GLSZM], gray-level dependence matrix [GLDM], and neighboring gray tone difference matrix [NGTDM]), were extracted from the original and filtered scans.

Lastly, the Wilcoxon rank-sum test was conducted to select optimized radiomic features, with a threshold set to $p < 0.01$. Then, multivariate logistic regression analysis was carried out to select significant features from the remaining radiomic features (features with $p < 0.05$ were retained). Finally, 16 radiomics features, including seven from edema areas and nine from hematoma areas, were selected as inputs for the edema and hematoma radiomics models. To explore the supplementary value of the edema region, we combined the radiomic features of the two regions and performed multivariate logistic regression analysis (the threshold set to $p < 0.05$) (Hematoma-Edema model). Ultimately, 12 features were selected as the input for the radiomic models (Fig. 2, Fig. S3, Table S1).

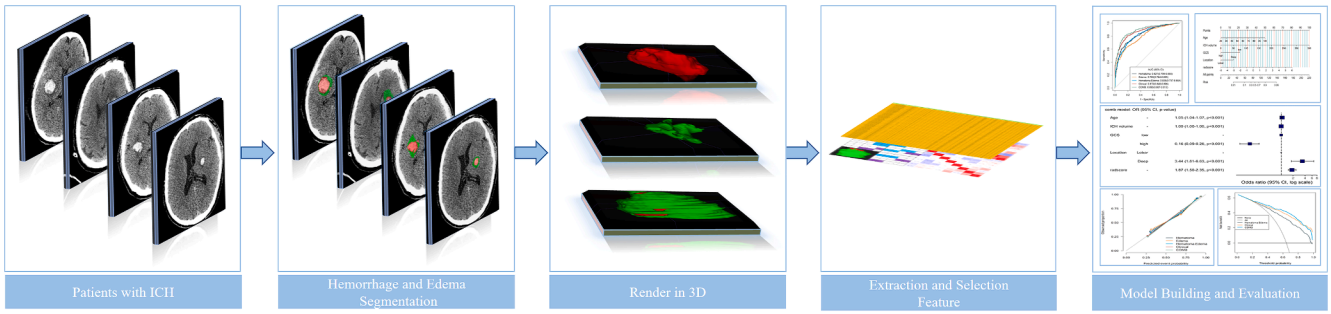


**Fig. 1. Workflow of the radiomics analysis pipeline.** Hematomas and perihematomal edemas manually segmented on non-contrast computed tomography (NCCT) images. Radiomic feature extraction and radiomics signature generation. Models are constructed, and their performance is assessed.

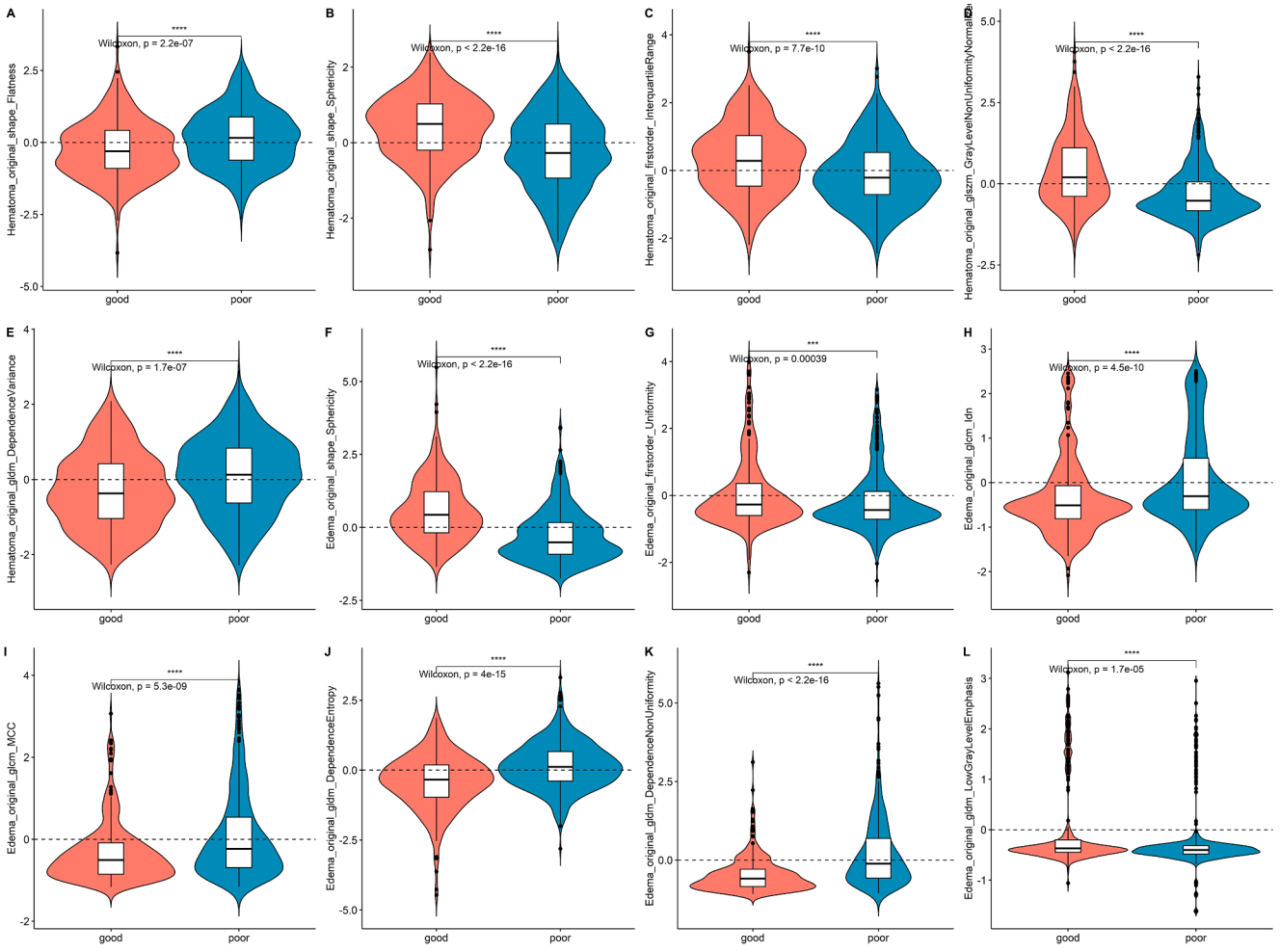


**Fig. 2. Violin plots.** The correlation between 12 radiomic features and characteristics of the good- and poor-outcome groups.

### *2.4. Model construction and validation*

For the clinical model, univariable analysis and multivariable logistic regression analysis were used to identify independent risk factors for poor outcome ($p < 0.05$). Next, independent risk factors were used to develop a clinical model using multivariable logistic regression analysis. For the radiomic model, the radiomic score (Rad-score) was converted to an outcome probability for each patient. The Rad-score was calculated as the corresponding non-zero coefficients of features selected from edema and/or hematoma by multivariate logistic regression in the training cohort. Three radiomic models were constructed using the Rad-score: the edema, hematoma, and hematoma-edema models. A combination model comprising the hematoma-edema Rad-score and clinical factors was also developed to assess the 3-month functional outcome of ICH patients in the training cohort. These models were then independently verified in the internal and external validation cohorts. To identify the best-performing model and the most discriminative features in the data set, we compared the areas under the receiving operating curve (AUC) of the models using the DeLong non-parametric approach. According to the integrated discrimination improvement (IDI) and net reclassification improvement (NRI), the model improvement after adding radiomic features was observed (Roscigno et al., 2021; Thomas et al.,

2019).

### 2.5. Statistical analysis

For clinical and laboratory data, quantitative variables were expressed as the median (interquartile range [IQR]), while categorical variables were reported as numbers and percentages as appropriate. The Mann–Whitney U, and chi-squared tests were used for univariate analysis, using $p < 0.05$ as the threshold for statistical significance. Multivariable logistic regression analysis was used to identify factors that were independently associated with functional outcomes and to construct the clinical model. For quantitative radiomic features, the Wilcoxon rank-sum test was used to choose the optimized features ($p < 0.01$). Multivariate logistic regression analysis was used to select significant features from the remaining features ($p < 0.05$). A receiver operating characteristic (ROC) curve was generated to determine model accuracy and discriminative performance. Sensitivity, specificity, accuracy, and AUC were used to estimate model performance. Calibration curves based on the Hosmer-Lemeshow test and decision curve analysis were used to compare the consistency and the clinical value of the models. The DeLong nonparametric approach, IDI, and NRI were used to compare performance differences among models and investigate radiomic markers to improve the identification of the outcome of patients with ICH. All statistical analyses were performed using R (version 4.1.0; R Foundation for Statistical Computing, Vienna, Austria) and SPSS (version 25; IBM, Armonk, NY).

## 3. Results

### 3.1. Patient characteristics

After applying the exclusion criteria, 2461 patients were excluded, the remaining 1098 patients were included. Among them, the median patient age was 60 years; there were 652 males and 446 females. The demographics, ICH characteristics on CT, risk factors for poor functional outcome, and results of univariate analysis are summarized in Table 1. In total, 703 patients had poor 3-month prognosis, with a high incidence of 64 %; the incidence of poor prognosis was similar across datasets. Patients with poor prognosis were significantly older than those with good functional outcome (median age, 60 years vs 56 years; $p < 0.001$); however, there was no significant difference in sex. Intraventricular hemorrhage and hypodensity sign were identified as risk factors of poor prognosis and found in 64 % and 73 % of patients, respectively. In addition, the presence of a midline shift >4 mm was closely related to hematoma and edema volumes and indicated poor prognosis. The laboratory indices related to poor prognosis included high glucose, neutrophil count, and neutrophil-lymphocyte ratio.

**Table 1**
Clinicodemographic patient characteristics.

| Parameter | Gansu training cohort | Gansu internal validation cohort | External validation cohort | All Data | | | |
|---|---|---|---|---|---|---|---|
| | *n* = 814 | *n* = 198 | *n* = 86 | | Poor outcome | Good outcome | *P* value [a] |
| Poor outcome* | 525 (65) | 129 (65) | 49 (57) | 703 (64) | 703 (64) | 395 (36) | |
| Time (h) | 3.0 (2.0, 4.0) | 2.8 (1.0, 4.0) | 2.5 (1.0, 4.0) | 3.0 (1.5, 4.0) | 3.0 (1.5, 4.0) | 3.0 (1.5, 4.0) | 0.41 |
| Gender* | | | | | | | 0.84 |
| Male | 465 (57) | 135 (68) | 52 (61) | 652 (59) | 419 (60) | 233 (59) | |
| Female | 349 (43) | 63 (32) | 34 (39) | 446 (41) | 284 (40) | 162 (41) | |
| Age (y) | 60 (52, 70) | 58 (51, 70) | 59 (53, 70) | 60 (52, 70) | 62 (53, 72) | 56 (50, 65) | < 0.001 |
| Location* | | | | | | | 0.32 |
| Deep | 727 (89) | 178 (90) | 72 (84) | 977 (89) | 629 (90) | 348 (88) | |
| Lobar | 87 (11) | 20 (10) | 14 (16) | 121 (11) | 74 (10) | 47 (12) | |
| Midline shift* | 224 (27) | 46 (23) | 12 (14) | 282 (26) | 254 (36) | 28 (7) | < 0.001 |
| IVH* | 409 (50) | 97 (49) | 40 (47) | 546 (50) | 449 (64) | 97 (25) | < 0.001 |
| SAH* | 151 (19) | 41 (21) | 16 (19) | 208 (19) | 181 (26) | 27 (7) | < 0.001 |
| Hypodensities* | 535 (66) | 145 (73) | 49 (57) | 729 (66) | 509 (72) | 220 (56) | < 0.001 |
| ICH volume ($mm^3$) | 29.8 (13.3, 69.8) | 32.9 (15.9, 76.2) | 43.8 (14.7, 67.2) | 31.1 (13.9, 70.5) | 51.7 (22.9, 90.5) | 16.4 (6.9, 27.3) | < 0.001 |
| PHE volume ($mm^3$) | 9.2 (4.1, 20.3) | 16.7 (7.6, 31.3) | 16.9 (7.3, 31.7) | 11.2 (4.9, 23.4) | 15.1(6.3, 29.9) | 6.5 (3.1, 13.3) | < 0.001 |
| Temperature (℃) | 36.6 (36.5, 36.9) | 36.5 (36.3, 36.7) | 36.5 (36.3, 36.6) | 36.6 (36.4, 36.8) | 36.6 (36.5, 36.8) | 36.5 (36.4, 36.8) | 0.01 |
| Smoking* | 133 (16) | 31 (16) | 25 (29) | 189 (17) | 126 (18) | 63 (16) | 0.53 |
| SBP (mmHg) | 171 (151, 190) | 174 (156, 195) | 175 (154, 192) | 172(153, 191) | 178 (156, 194) | 166 (149, 185) | < 0.001 |
| GCS* | | | | | | | < 0.001 |
| Low (score < 9) | 301 (37) | 68 (34) | 30 (35) | 399 (36) | 365 (52) | 34 (9) | |
| High (score ≥ 9) | 513 (63) | 130 (66) | 56 (65) | 699 (64) | 338 (48) | 361 (91) | |
| GLU (mmol/L) | 7.92 (6.44, 10.10) | 7.72 (6.28, 9.75) | 8.12 (6.15, 9.12) | 7.90 (6.40, 9.89) | 8.50 (6.85, 10.71) | 6.82 (5.93, 8.51) | < 0.001 |
| TG (mmol/L) | 1.28 (0.82, 2.15) | 1.09 (0.66, 1.76) | 1.46 (1.07, 1.84) | 1.26 (0.99, 1.99) | 1.30 (0.85, 2.02) | 1.23 (0.74, 1.91) | 0.10 |
| WBC (10^9/L) | 8.56 (6.30, 11.65) | 8.12 (6.40, 11.46) | 10.27 (6.90, 13.88) | 8.61 (6.38, 11.79) | 9.31 (6.80, 12.95) | 7.49 (5.72, 10.02) | < 0.001 |
| NE (10^9/L) | 6.93 (4.46, 9.99) | 6.28 (4.30, 9.79) | 8.31 (5.07, 12.18) | 6.94 (4.46, 10.10) | 7.52 (4.79, 11.08) | 5.59 (4.07, 8.56) | < 0.001 |
| LY (10^9/L) | 1.02 (0.69, 1.57) | 1.12 (0.69, 1.76) | 1.12 (0.83, 1.59) | 1.04 (0.70, 1.60) | 1.06 (0.67, 1.64) | 1.02 (0.76, 1.53) | 0.85 |
| NLR | 6.24 (3.39, 12.34) | 5.93 (2.69, 11.60) | 7.68 (3.99, 13.29) | 6.25 (3.35, 12.25) | 7.51 (3.56, 13.65) | 5.25 (3.15, 9.79) | < 0.001 |
| HGB (g/L) | 148 (137, 161) | 151 (139, 164) | 141 (129, 154) | 148 (136, 161) | 149 (137, 162) | 147 (136, 158) | 0.09 |
| INR | 0.98 (0.93, 1.04) | 1.02 (0.97, 1.06) | 1.04 (0.95, 1.06) | 0.99 (0.94, 1.05) | 0.99 (0.94, 1.05) | 0.99 (0.93, 1.05) | 0.31 |

Data are presented as the median (interquartile range) unless otherwise indicated. Time = time from symptom onset to baseline CT, IVH = intraventricular hemorrhage, SAH = subarachnoid hemorrhage, ICH = intracerebral hemorrhage, PHE = perihematomal edema, SBP = systolic blood pressure, GCS = Glasgow Coma Scale, GLU = glucose, TG = triglycerides, WBC = white blood cell, NE = neutrophil, LY = lymphocyte, NLR = neutrophil-lymphocyte ratio, HGB = hemoglobin, INR = international normalized ratio.

* Data are presented as n (%).

[a] P-values were obtained using chi-square tests for categorical variables, and Mann-Whitney U-tests for continuous variables.

### 3.2. Model comparison and final model

The edema, hematoma, hematoma-edema, clinical, and combined models are depicted in Fig. 3. These models showed an AUCs of 0.795 (95 % confidence interval [CI] = 0.764–0.825), 0.827 (95 % CI = 0.798–0.855), 0.826 (95 % CI = 0.797–0.854), 0.872 (95 % CI = 0.848–0.896), and 0.890 (95 % CI = 0.867–0.912), respectively, in the training cohort. The individual AUC, accuracy sensitivity, specificity, and positive and negative predictive values in the training, internal validation, and external validation cohorts are reported in Table 2. The consistency between predicted and actual poor functional prognosis at 3 months evaluated by the calibration curve (Hosmer-Lemeshow test; Fig. 4A–C) indicated good agreement among the cohorts.

For clinical utility, the decision curve (Fig. 4D–F) showed that the combined model (light blue) had better predictive capability for poor outcomes than the Rad-score or clinical model alone (dark green and orange, respectively). There was no significant difference in AUCs between the hematoma and edema models, indicating similar prediction abilities. However, there were significant differences in AUCs between the hematoma and combined models and between the hematoma-edema and combined models in the three cohorts ($p < 0.05$, DeLong test; Table S2). In addition, after incorporating radiomics features, the combined model showed better performance than the clinical models: the NRI was 0.140 (95 % CI = 0.073–0.206), 0.165 (95 % CI = 0.037–0.292), and 0.196 (95 % CI = 0.013–0.379), and the IDI was 0.050 (95 % CI = 0.036–0.064), 0.034 (95 % CI = 0.005–0.063), and 0.066 (95 % CI = 0.032–0.101) in the training, internal validation, and external validation datasets, respectively (Table 3).

These findings indicate that radiomics has additional value in predicting the prognosis of ICH patients at 3 months. When comparing the predictive performance of the models, the combination model comprising the hematoma-edema Rad-score and clinical factors performed the best. This model included the risk factors of age (odds ratio [OR], 1.05; 95 % CI = 1.04–1.07; $p < 0.001$), ICH volume (OR, 1.00; 95 % CI = 1.00–1.00; $p < 0.001$), GCS score (OR, 0.16; 95 % CI = 0.09–0.28; $p < 0.001$), hemorrhage location (OR, 3.44; 95 % CI = 1.81–6.63; $p < 0.001$), and hematoma-edema Rad-score (OR, 1.87; 95 % CI = 1.50–2.35; $p < 0.001$), all of which were significantly associated with 3-month outcomes in all three cohorts (Fig. 5A). We plotted a nomogram by using these risk markers to visualize the combined model (Fig. 5B).

## 4. Discussion

Although recent studies demonstrate that radiomics models can predict functional outcomes in ICH, these studies were either relatively small or their accuracy and stability were insufficient (Pszczolkowski et al., 2021; Song et al., 2021). Herein, a model based on clinical and radiomic features of hematoma and PHE area on NCCT imaging accurately predicted 3-month outcomes of patients with ICH. The radiomic features of the hematoma and PHE areas on NCCT imaging could quantify the shape and heterogeneity of hematomas and edema. The addition of the Rad-score to the clinical model increased model accuracy, sensitivity, and specificity, providing additional information for ICH outcome prediction.

Accurate prognosis risk stratification in patients with ICH is key to implementing effective interventions and improving patient cooperation with respect to active rehabilitation. For example, rapid stratification of patients with ICH in the ultra-early and targeted therapeutic interventions (such as intensive blood pressure reduction) can improve the functional outcome(Li et al., 2020). Our findings are consistent with previous findings indicating that conventional markers, such as age, hematoma volume and location, and GCS score, are more specific than sensitive for outcome prediction (Haupenthal et al., 2021; Nawabi et al., 2021; Pasi et al., 2021). A larger hematoma volume is associated with greater mass effect, more neuron damage, and lower GCS score, all of which are related to worse outcomes. A deep hematoma is a high risk factor for poor prognosis owing to its close relationship with important neural structures, and thalamic ICHs have a high probability of intraventricular extension and brainstem compression (Eslami et al., 2019). Further, compared with lobar locations, deep locations have a higher density of corticospinal tracts. As lower hematoma volume or hemorrhage expansion has greater impacts on clinical outcome (Roh et al., 2020), we included hematoma location in the final model, even though it was not significant in univariate analysis. Older age also increases the risk of recurrent ICH due to greater use of antithrombotic agents and prevalence of cerebral amyloid angiopathy and lower social support, which contribute to worse prognosis (Rådholm et al., 2015). In addition, older patients usually have other chronic diseases, such as diabetes or heart disease, which limit ICH recovery to some extent.

Analyzing pathological changes in the hematoma and PHE may provide more information for the effective treatment of ICH. In the past two decades, the relationship between different hematoma shapes or density on NCCT images and prognosis has been repeatedly investigated. However, these visual signs are vaguely named and their predictive accuracy is affected by interobserver consistency (Morotti et al., 2019). PHE formation is considered a quantitative marker of secondary injury; its occurrence and development are accompanied by complex pathological changes. Moreover, the impact of PHE on clinical results is unclear (Chen et al., 2021). Compared with radiological signs, radiomics features reflect the morphological and density characteristics of VOI's (Zwanenburg et al., 2020a), providing a more quantitative and

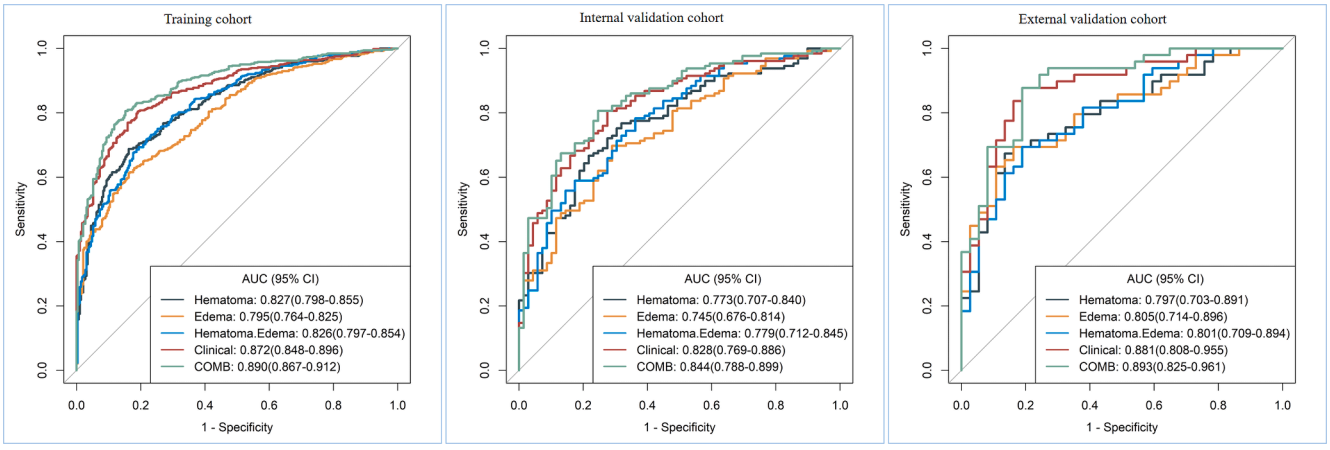


**Fig. 3. Receiver operating characteristic curves.** Receiver operating characteristic curves of the five models for assessing 3-month clinical functional outcome in the three cohorts.

**Table 2**
Model performance.

| | | Hematoma | Edema | Hematoma-Edema | Clinical | COMB |
|---|---|---|---|---|---|---|
| | Cut off | 0.662 | 0.713 | 0.658 | 0.550 | 0.608 |
| Training cohort | AUC | 0.827(0.798–0.855) | 0.795(0.764–0.825) | 0.826(0.797–0.854) | 0.872(0.848–0.896) | 0.890(0.867–0.912) |
| | Accuracy | 0.741(0.709–0.771) | 0.693(0.660–0.724) | 0.741(0.709–0.771) | 0.800(0.771–0.827) | 0.816(0.787–0.842) |
| | Sensitivity | 0.688(0.604–0.735) | 0.613(0.533–0.653) | 0.718(0.653–0.770) | 0.781(0.709–0.815) | 0.802(0.739–0.838) |
| | Specificity | 0.837(0.744–0.879) | 0.837(0.772–0.882) | 0.782(0.723–0.830) | 0.834(0.744–0.875) | 0.841(0.765–0.882) |
| | PPV | 0.885(0.871–0.891) | 0.873(0.856–0.879) | 0.857(0.845–0.865) | 0.895(0.886–0.899) | 0.901(0.894–0.905) |
| | NPV | 0.596(0.567–0.608) | 0.544(0.523–0.557) | 0.604(0.585–0.619) | 0.677(0.651–0.688) | 0.700(0.680–0.710) |
| Internal validation cohort | AUC | 0.773(0.707–0.840) | 0.745(0.676–0.814) | 0.779(0.712–0.845) | 0.828(0.769–0.886) | 0.844(0.788–0.899) |
| | Accuracy | 0.712(0.644–0.774) | 0.646(0.576–0.713) | 0.707(0.638–0.769) | 0.753(0.686–0.811) | 0.763(0.697–0.820) |
| | Sensitivity | 0.705(0.511–0.814) | 0.589(0.449–0.737) | 0.713(0.550–0.822) | 0.767(0.612–0.907) | 0.775(0.666–0.891) |
| | Specificity | 0.725(0.593–0.855) | 0.754(0.652–0.870) | 0.696(0.550–0.812) | 0.725(0.638–0.812) | 0.739(0.609–0.855) |
| | PPV | 0.827(0.776–0.847) | 0.817(0.773–0.848) | 0.814(0.772–0.835) | 0.839(0.806–0.860) | 0.847(0.827–0.865) |
| | NPV | 0.568(0.519–0.608) | 0.495(0.459–0.531) | 0.565(0.507–0.602) | 0.625(0.595–0.651) | 0.638(0.592–0.671) |
| External validation cohort | AUC | 0.797(0.703–0.891) | 0.805(0.714–0.896) | 0.801(0.709–0.894) | 0.881(0.808–0.955) | 0.893(0.825–0.961) |
| | Accuracy | 0.756(0.651–0.842) | 0.744(0.639–0.832) | 0.733(0.626–0.822) | 0.802(0.702–0.880) | 0.837(0.742–0.908) |
| | Sensitivity | 0.673(0.326–0.817) | 0.694(0.510–0.837) | 0.694(0.510–0.837) | 0.878(0.735–0.980) | 0.878(0.571–0.980) |
| | Specificity | 0.865(0.594–0.973) | 0.811(0.541–0.947) | 0.784(0.486–0.919) | 0.703(0.432–0.865) | 0.784(0.432–0.919) |
| | PPV | 0.868(0.762–0.889) | 0.829(0.781–0.854) | 0.810(0.757–0.837) | 0.796(0.766–0.814) | 0.843(0.778–0.857) |
| | NPV | 0.667(0.579–0.692) | 0.667(0.571–0.700) | 0.659(0.545–0.694) | 0.812(0.727–0.842) | 0.829(0.727–0.850) |

COMB = combined model, AUC = area under the receiver operating characteristic curve, PPV = positive predictive value, NPV = negative predictive value. Data in parenthesis indicate 95 % confidence intervals.

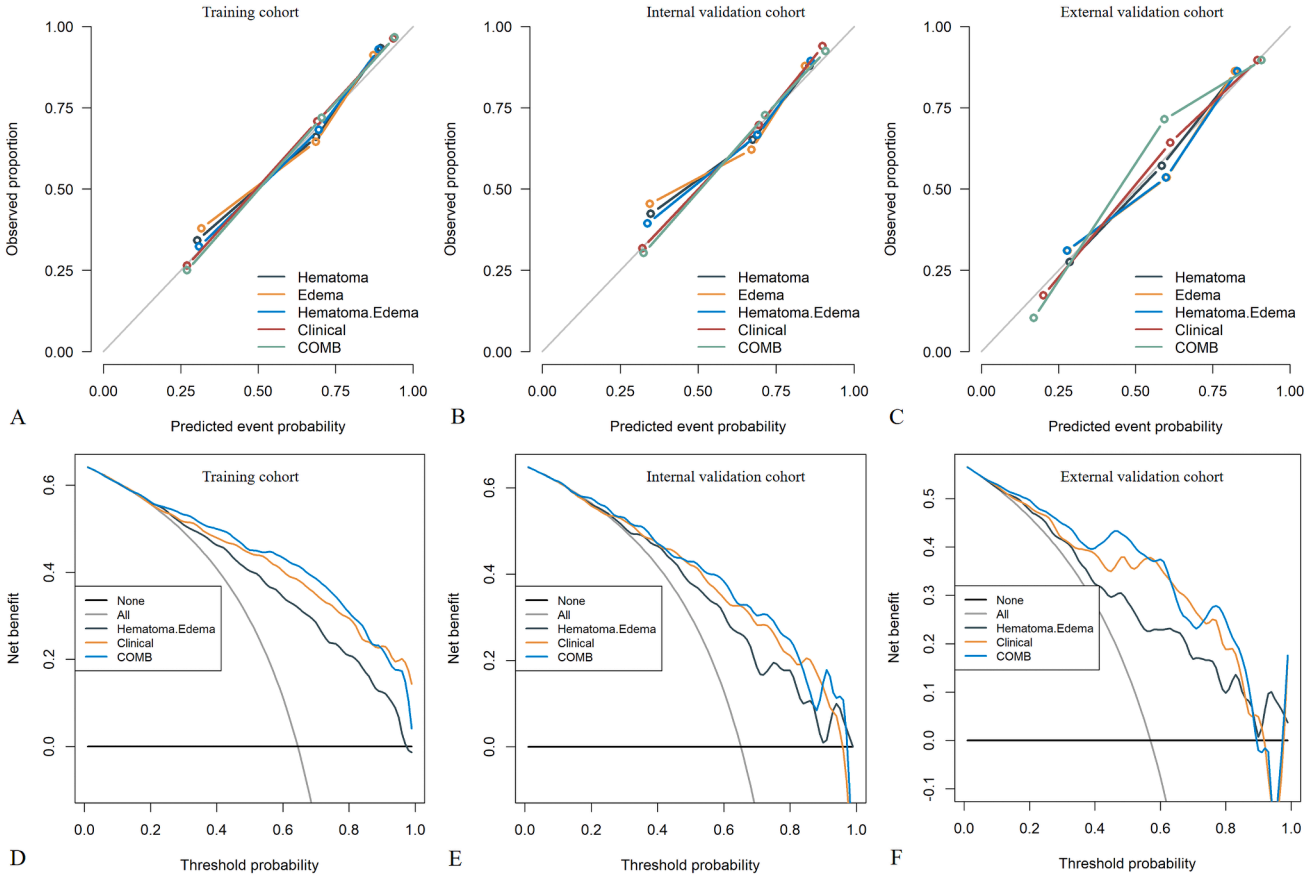


**Fig. 4. Calibration curves and Decision curves.** (A-C) Calibration curves of the models for predicting poor outcome at 3 months in the three cohorts. The poor outcomes are plotted on the y-axis; model-predicted probability is plotted on the x-axis. (D-F) Decision curve analysis for the models in the three cohorts. The gray line represents the assumption that all patients developed a poor outcome, and the black line represents the assumption that no patient had a poor outcome. The model with the highest curve and greater area was selected as the optimal model for decision making, with maximal net benefit in outcome prediction.

**Table 3**
NRI and IDI of the predictive models.

| Clinical vs COMB | NRI | *P* value | IDI | *P* value |
|---|---|---|---|---|
| Training cohort | 0.140 (0.073–0.206) | <0.001 | 0.050 (0.036–0.064) | <0.001 |
| Internal validation cohort | 0.165 (0.037–0.292) | 0.01 | 0.034 (0.005–0.063) | 0.02 |
| External validation cohort | 0.196 (0.013–0.379) | 0.04 | 0.066 (0.032–0.101) | <0.001 |

NRI = net reclassification improvement, IDI = integrated discrimination improvement, Clinical = clinical model, COMB = combined model.
Data in parenthesis indicate 95% confidence intervals.

consistent method to address the heterogeneity in hematoma and PHE. Moreover, these features have good predictive value for hematoma expansion and poor functional outcome, yielding better sensitivity and AUC (Haider et al., 2021; Nawabi et al., 2021; Pszczolkowski et al., 2021; Song et al., 2021). The results herein indicated that radiomic features of the hematoma and PHE area, including shape and first-, second-, and high-order features (GLCM, GLRLM, GLSZM, GLDM, NGTDM), were associated with prognosis. These features enable comprehensive quantification of pathological changes in hematoma and PHE. For instance, shape features—an objective and quantitative index—can describe the three-dimensional size and morphology of the hematoma and PHE; first-, second-, and high-order features can reflect the spatial arrangement of gray- level image voxel. This is consistent with previous studies that predicted prognosis based on shape and density characteristics, but goes even further.

According to the results of previous radiomics studies related to cancer (Su et al., 2020; Tomita et al., 2021), the radiomics features not only reflect the presence of active bleeding and time course of bleeding, but may also reflect microglia/macrophage activation and neuro-inflammation in the hemorrhage and PHE areas. A comparison of selected radiomic features showed no significant differences in AUC values, specificity, and sensitivity among the Rad-score model of the hematoma area, the PHE area alone, and the hematoma-edema Rad-score model. This may prove that the pathological changes of primary and secondary injuries are similarly important in determining ICH prognosis. In contrast, the effect of perihematomal edema on prognosis appears more complex. The hematoma-edema Rad-score and clinical models showed similar predictive accuracy. Importantly, the predictive performance of the clinical model significantly improved with the addition of radiomic features. These findings support the hypothesis that radiomic features could better reflect ICH pathophysiology and provide accurate prognostic information. These pathological changes may be potential therapeutic targets for intracerebral hemorrhage in the future.

Nonetheless, there are several limitations to our study. First, it was based on retrospective data; outcomes could be influenced by changes in the level of care post-ICH (e.g., withdrawal of care in some patients), potentially affecting outcome data. Second, patient enrollment was disproportionate; center1 was a local stroke center and other centers' Picture Archiving and Communication Systems could not read earlier information. Third, the inclusion criteria were a 6-h window between symptom onset and baseline CT and excluded patients without PHE; however, many patients were admitted >6 h after symptom onset or there may have been no obvious PHE within 6 h, limiting the scope of model application. Fourth, although quantitative radiomic features could accurately predict prognosis and provide additional value, combining these radiomics features with physiopathology was challenging. Future research should clarify the biological mechanisms underlying the prognostic influence of the quantitative radiomic features of hematoma and PHE to establish more effective treatment modalities for ICH.

## 5. Conclusion

In this retrospective, multicenter study, we evaluated the role and accuracy of radiomic features in predicting ICH prognosis. We demonstrated that radiomic features can quantitatively analyze morphological features and the internal heterogeneity of the hematoma and edema area, providing additional value in prognostic prediction and risk stratification. Similar to clinical features, the radiomic features of PHE were also associated with prognosis. This simple and easy-to-use nomogram scoring system can help clinicians perform rapid and objective functional outcome stratification and make rational clinical treatment decisions.

**Ethical approval**.

Ethical approval was obtained from the Lanzhou University Second Hospital, Gansu Provincial Hospital, and Xi'an Central Hospital institutional review boards (Approval number: 2022A-096, 2022–275 and LW-2022–011).

## CRediT authorship contribution statement

**Xiaoyu Huang:** Conceptualization, Formal analysis, Investigation, Methodology, Software, Visualization, Writing – original draft, Writing – review & editing. **Dan Wang:** Conceptualization, Formal analysis, Investigation, Methodology, Software, Visualization, Writing – original draft, Writing – review & editing. **Qiaoying Zhang:** Data curation. **Yaqiong Ma:** Data curation. **Hui Zhao:** Data curation. **Shenglin Li:** Data curation. **Juan Deng:** Data curation. **Jialiang Ren:** Formal analysis, Methodology, Software, Visualization, Writing – original draft, Writing – review & editing. **Jingjing Yang:** Data curation. **Zhiyong Zhao:** Data curation. **Min Xu:** Data curation. **Qing Zhou:** Data curation. **Junlin Zhou:** Conceptualization, Methodology, Supervision, Writing – review & editing.

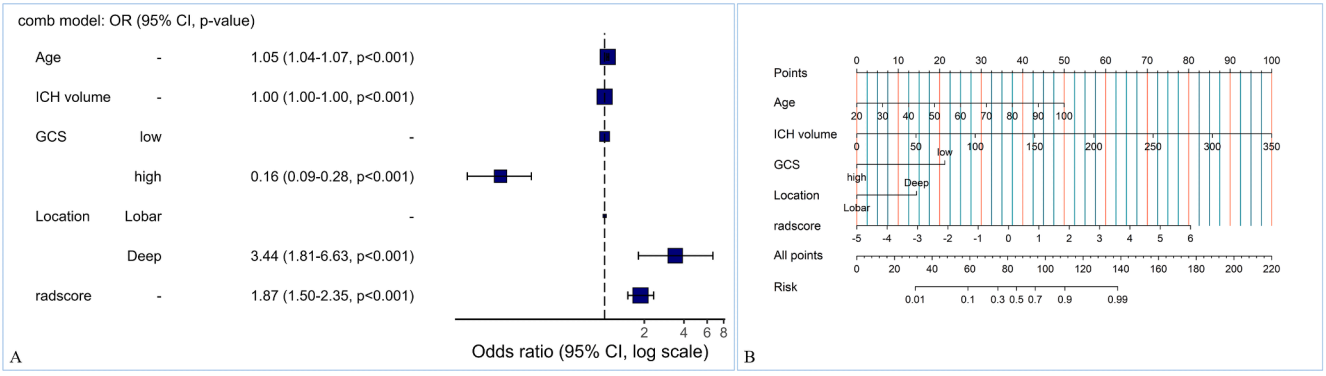


**Fig. 5. Forest plot and Nomogram.** (A) Forest plot showing multivariate association between 3-month functional outcome and clinical and radiomic characteristics. (B) Nomogram to predict 3-month clinical functional outcomes. GCS = Glasgow Coma Scale.

## Declaration of Competing Interest

The authors declare that they have no known competing financial interests or personal relationships that could have appeared to influence the work reported in this paper.

## Data availability

Data will be made available on request.

*Acknowledgments*

We thank Yijing Xie, Huaze Xi, Hongyu Zhang, Long Yuan, Fukai Li providing assistance with data collection and maintenance.

*Funding acknowledgments*

This study was funded by Grant Nos. 82071872 from National Natural Science Foundation of China, and Grant Nos. 21YF5FA123 from Science and Technology Program Funding Project of Gansu Province.

*Disclosures*

The authors have no conflicts of interest to disclose. The corresponding author (JLZ) had full access to all the data in the study and takes responsibility for its integrity and the data analysis.

## Appendix A. Supplementary data

Supplementary data to this article can be found online at https://doi.org/10.1016/j.nicl.2022.103242.

## References

The top 10 causes of death [WWW Document], n.d. URL https://www.who.int/news-room/fact-sheets/detail/the-top-10-causes-of-death (accessed 12.28.21).

Andersen, K.K., Olsen, T.S., Dehlendorff, C., Kammersgaard, L.P., 2009. Hemorrhagic and ischemic strokes compared: stroke severity, mortality, and risk factors. Stroke 40, 2068–2072. https://doi.org/10.1161/STROKEAHA.108.540112.

Babi, M.-A., James, M.L., 2017. Peri-Hemorrhagic Edema and Secondary Hematoma Expansion after Intracerebral Hemorrhage: From Benchwork to Practical Aspects. Front Neurol 8, 4. https://doi.org/10.3389/fneur.2017.00004.

Barras, C.D., Tress, B.M., Christensen, S., MacGregor, L., Collins, M., Desmond, P.M., Skolnick, B.E., Mayer, S.A., Broderick, J.P., Diringer, M.N., Steiner, T., Davis, S.M., Factor, R.A., Intracerebral Hemorrhage Trial Investigators, V.I.I., 2009. Density and shape as CT predictors of intracerebral hemorrhage growth. Stroke 40, 1325–1331. https://doi.org/10.1161/STROKEAHA.108.536888.

Boulouis, G., Morotti, A., Brouwers, H.B., Charidimou, A., Jessel, M.J., Auriel, E., Pontes-Neto, O., Ayres, A., Vashkevich, A., Schwab, K.M., Rosand, J., Viswanathan, A., Gurol, M.E., Greenberg, S.M., Goldstein, J.N., 2016. Association Between Hypodensities Detected by Computed Tomography and Hematoma Expansion in Patients With Intracerebral Hemorrhage. JAMA Neurol 73, 961–968. https://doi.org/10.1001/jamaneurol.2016.1218.

Chen, Y., Chen, S., Chang, J., Wei, J., Feng, M., Wang, R., 2021. Perihematomal Edema After Intracerebral Hemorrhage: An Update on Pathogenesis, Risk Factors, and Therapeutic Advances. Front Immunol 12, 740632. https://doi.org/10.3389/fimmu.2021.740632.

Eslami, V., Tahsili-Fahadan, P., Rivera-Lara, L., Gandhi, D., Ali, H., Parry-Jones, A., Nelson, L.S., Thompson, R.E., Nekoobakht-Tak, S., Dlugash, R., McBee, N., Awad, I., Hanley, D.F., Ziai, W.C., 2019. Influence of Intracerebral Hemorrhage Location on Outcomes in Patients With Severe Intraventricular Hemorrhage. Stroke 50 (7), 1688–1695.

Ferro, J.M., Canhão, P., Stam, J., Bousser, M.-G., Barinagarrementeria, F., Investigators, I.S.C.V.T., 2004. Prognosis of cerebral vein and dural sinus thrombosis: results of the International Study on Cerebral Vein and Dural Sinus Thrombosis (ISCVT). Stroke 35, 664–670. https://doi.org/10.1161/01.STR.0000117571.76197.26.

GBD 2016 Neurology Collaborators, 2019. Global, regional, and national burden of neurological disorders, 1990-2016: a systematic analysis for the Global Burden of Disease Study 2016. Lancet Neurol 18, 459–480. https://doi.org/10.1016/S1474-4422(18)30499-X.

Greenberg, S.M., Ziai, W.C., Cordonnier, C., Dowlatshahi, D., Francis, B., Goldstein, J.N., Hemphill, J.C., Johnson, R., Keigher, K.M., Mack, W.J., Mocco, J., Newton, E.J., Ruff, I.M., Sansing, L.H., Schulman, S., Selim, M.H., Sheth, K.N., Sprigg, N., Sunnerhagen, K.S., Association, A.H., Association, A.S., 2022. 2022 Guideline for the Management of Patients With Spontaneous Intracerebral Hemorrhage: A Guideline From the American Heart Association/American Stroke Association. Stroke 53, e282–e361. https://doi.org/10.1161/STR.0000000000000407.

Haider, S.P., Qureshi, A.I., Jain, A., Tharmaseelan, H., Berson, E.R., Zeevi, T., Majidi, S., Filippi, C.G., Iseke, S., Gross, M., Acosta, J.N., Malhotra, A., Kim, J.A., Sansing, L.H., Falcone, G.J., Sheth, K.N., Payabvash, S., 2021. Admission computed tomography radiomic signatures outperform hematoma volume in predicting baseline clinical severity and functional outcome in the ATACH-2 trial intracerebral hemorrhage population. Eur J Neurol 28, 2989–3000. https://doi.org/10.1111/ene.15000.

Haupenthal, D., Kuramatsu, J.B., Volbers, B., Sembill, J.A., Mrochen, A., Balk, S., Hoelter, P., Lücking, H., Engelhorn, T., Dörfler, A., Schwab, S., Huttner, H.B., Sprügel, M.I., 2021. Disability-Adjusted Life-Years Associated With Intracerebral Hemorrhage and Secondary Injury. JAMA Netw Open 4 (7), e2115859.

Ironside, N., Chen, C.-J., Ding, D., Mayer, S.A., Connolly, E.S., 2019. Perihematomal Edema After Spontaneous Intracerebral Hemorrhage. Stroke 50 (6), 1626–1633.

Kniep, H.C., Madesta, F., Schneider, T., Hanning, U., Schönfeld, M.H., Schön, G., Fiehler, J., Gauer, T., Werner, R., Gellissen, S., 2019. Radiomics of Brain MRI: Utility in Prediction of Metastatic Tumor Type. Radiology 290, 479–487. https://doi.org/10.1148/radiol.2018180946.

Li, Q., Liu, Q.-J., Yang, W.-S., Wang, X.-C., Zhao, L.-B., Xiong, X., Li, R., Cao, D., Zhu, D., Wei, X., Xie, P., 2017. Island Sign: An Imaging Predictor for Early Hematoma Expansion and Poor Outcome in Patients With Intracerebral Hemorrhage. Stroke 48, 3019–3025. https://doi.org/10.1161/STROKEAHA.117.017985.

Li, Q., Yang, W.-S., Chen, S.-L., Lv, F.-R., Lv, F.-J., Hu, X., Zhu, D., Cao, D., Wang, X.-C., Li, R., Yuan, L., Qin, X.-Y., Xie, P., 2018. Black Hole Sign Predicts Poor Outcome in Patients with Intracerebral Hemorrhage. Cerebrovasc Dis 45, 48–53. https://doi.org/10.1159/000486163.

Li, Q., Warren, A.D., Qureshi, A.I., Morotti, A., Falcone, G.J., Sheth, K.N., Shoamanesh, A., Dowlatshahi, D., Viswanathan, A., Goldstein, J.N., 2020. Ultra-Early Blood Pressure Reduction Attenuates Hematoma Growth and Improves Outcome in Intracerebral Hemorrhage. Ann Neurol 88, 388–395. https://doi.org/10.1002/ana.25793.

Li, Q.i., Zhang, G., Huang, Y.-J., Dong, M.-X., Lv, F.-J., Wei, X., Chen, J.-J., Zhang, L.-J., Qin, X.-Y., Xie, P., 2015. Blend Sign on Computed Tomography: Novel and Reliable Predictor for Early Hematoma Growth in Patients With Intracerebral Hemorrhage [WWW Document]. Stroke 46 (8), 2119–2123.

Morotti, A., Boulouis, G., Dowlatshahi, D., Li, Q.i., Barras, C.D., Delcourt, C., Yu, Z., Zheng, J., Zhou, Z., Aviv, R.I., Shoamanesh, A., Sporns, P.B., Rosand, J., Greenberg, S.M., Al-Shahi Salman, R., Qureshi, A.I., Demchuk, A.M., Anderson, C.S., Goldstein, J.N., Charidimou, A., 2019. Standards for Detecting, Interpreting, and Reporting Noncontrast Computed Tomographic Markers of Intracerebral Hemorrhage Expansion. Ann Neurol 86 (4), 480–492.

Morotti, A., Arba, F., Boulouis, G., Charidimou, A., 2020. Noncontrast CT markers of intracerebral hemorrhage expansion and poor outcome: A meta-analysis. Neurology 95, 632–643. https://doi.org/10.1212/WNL.0000000000010660.

Nawabi, J., Kniep, H., Elsayed, S., Friedrich, C., Sporns, P., Rusche, T., Böhmer, M., Morotti, A., Schlunk, F., Dührsen, L., Broocks, G., Schön, G., Quandt, F., Thomalla, G., Fiehler, J., Hanning, U., 2021. Imaging-Based Outcome Prediction of Acute Intracerebral Hemorrhage. Transl Stroke Res 12 (6), 958–967.

Pasi, M., Casolla, B., Kyheng, M., Boulouis, G., Kuchcinski, G., Moulin, S., Labreuche, J., Henon, H., Leys, D., Cordonnier, C., 2021. Long-term functional decline of spontaneous intracerebral haemorrhage survivors. J Neurol Neurosurg Psychiatry 92, 249–254. https://doi.org/10.1136/jnnp-2020-324741.

Pszczolkowski, S., Manzano-Patrón, J.P., Law, Z.K., Krishnan, K., Ali, A., Bath, P.M., Sprigg, N., Dineen, R.A., 2021. Quantitative CT radiomics-based models for prediction of haematoma expansion and poor functional outcome in primary intracerebral haemorrhage. Eur Radiol 31, 7945–7959. https://doi.org/10.1007/s00330-021-07826-9.

Rådholm, K., Arima, H., Lindley, R.I., Wang, J., Tzourio, C., Robinson, T., Heeley, E., Anderson, C.S., Chalmers, J., INTERACT2 Investigators,, 2015. Older age is a strong predictor for poor outcome in intracerebral haemorrhage: the INTERACT2 study. Age Ageing 44, 422–427. https://doi.org/10.1093/ageing/afu198.

Roh, D., Boehme, A., Young, C., Roth, W., Gutierrez, J., Flaherty, M., Rosand, J., Testai, F., Woo, D., Elkind, M.S.V., 2020. Hematoma expansion is more frequent in deep than lobar intracerebral hemorrhage. e3393 Neurology 95, e3386. https://doi.org/10.1212/WNL.0000000000010990.

Roscigno, G., Quintavalle, C., Biondi-Zoccai, G., De Micco, F., Frati, G., Affinito, A., Nuzzo, S., Condorelli, G., Briguori, C., 2021. Urinary Dickkopf-3 and Contrast-Associated Kidney Damage. J Am Coll Cardiol 77, 2667–2676. https://doi.org/10.1016/j.jacc.2021.03.330.

Serrano, E., López-Rueda, A., Moreno, J., Rodríguez, A., Llull, L., Zwanzger, C., Oleaga, L., Amaro, S., 2022. The new Hematoma Maturity Score is highly associated with poor clinical outcome in spontaneous intracerebral hemorrhage. Eur Radiol 32, 290–299. https://doi.org/10.1007/s00330-021-08085-4.

Shoamanesh, A., Morotti, A., Romero, J.M., Oliveira-Filho, J., Schlunk, F., Jessel, M.J., Ayres, A.M., Vashkevich, A., Schwab, K., Afzal, M.R., Cassarly, C., Martin, R.H., Qureshi, A.I., Greenberg, S.M., Rosand, J., Goldstein, J.N., Treatment, A., of Acute Cerebral Hemorrhage 2 (ATACH-2) and the Neurological Emergencies Treatment Trials (NETT) Network Investigators,, 2018. Cerebral Microbleeds and the Effect of Intensive Blood Pressure Reduction on Hematoma Expansion and Functional Outcomes: A Secondary Analysis of the ATACH-2 Randomized Clinical Trial. JAMA Neurol 75, 850–859. https://doi.org/10.1001/jamaneurol.2018.0454.

Skajaa, N., Adelborg, K., Horváth-Puhó, E., Rothman, K.J., Henderson, V.W., Thygesen, L.C., Sørensen, H.T., 2022. Stroke and Risk of Mental Disorders Compared With Matched General Population and Myocardial Infarction Comparators. Stroke STROKEAHA121037740. Stroke 53 (7), 2287–2298.

Song, Z., Tang, Z., Liu, H., Guo, D., Cai, J., Zhou, Z., 2021. A clinical-radiomics nomogram may provide a personalized 90-day functional outcome assessment for spontaneous intracerebral hemorrhage. Eur Radiol 31, 4949–4959. https://doi.org/10.1007/s00330-021-07828-7.

Sprügel, M.I., Kuramatsu, J.B., Volbers, B., Gerner, S.T., Sembill, J.A., Madžar, D., Bobinger, T., Kölbl, K., Hoelter, P., Lücking, H., Dörfler, A., Schwab, S., Huttner, H. B., 2019. Perihemorrhagic edema: Revisiting hematoma volume, location, and surface. e1170 Neurology 93, e1159. https://doi.org/10.1212/WNL.0000000000008129.

Su, X., Chen, N., Sun, H., Liu, Y., Yang, X., Wang, W., Zhang, S., Tan, Q., Su, J., Gong, Q., Yue, Q., 2020. Automated machine learning based on radiomics features predicts H3 K27M mutation in midline gliomas of the brain. Neuro Oncol 22, 393–401. https://doi.org/10.1093/neuonc/noz184.

Tan, C.O., Lam, S., Kuppens, D., Bergmans, R.H.J., Parameswaran, B.K., Forghani, R., Hu, R., Daftari Besheli, L., Goldstein, J.N., Thrall, J., Lev, M., Romero, J.M., Gupta, R., 2019. Spot and Diffuse Signs: Quantitative Markers of Intracranial Hematoma Expansion at Dual-Energy CT. Radiology 290, 179–186. https://doi.org/10.1148/radiol.2018180322.

Thomas, L.E., O'Brien, E.C., Piccini, J.P., D'Agostino, R.B., Pencina, M.J., 2019. Application of net reclassification index to non-nested and point-based risk prediction models: a review. Eur Heart J 40, 1880–1887. https://doi.org/10.1093/eurheartj/ehy345.

Tomita, H., Yamashiro, T., Heianna, J., Nakasone, T., Kimura, Y., Mimura, H., Murayama, S., 2021. Nodal-based radiomics analysis for identifying cervical lymph node metastasis at levels I and II in patients with oral squamous cell carcinoma using contrast-enhanced computed tomography. Eur Radiol 31, 7440–7449. https://doi.org/10.1007/s00330-021-07758-4.

Wu, T.Y., Sharma, G., Strbian, D., Putaala, J., Desmond, P.M., Tatlisumak, T., Davis, S. M., Meretoja, A., 2017. Natural History of Perihematomal Edema and Impact on Outcome After Intracerebral Hemorrhage. Stroke 48, 873–879. https://doi.org/10.1161/STROKEAHA.116.014416.

Yang, J., Arima, H., Wu, G., Heeley, E., Delcourt, C., Zhou, J., Chen, G., Wang, X., Zhang, S., Yu, S., Chalmers, J., Anderson, C.S., 2015. Prognostic significance of perihematomal edema in acute intracerebral hemorrhage: pooled analysis from the intensive blood pressure reduction in acute cerebral hemorrhage trial studies. Stroke 46, 1009–1013. https://doi.org/10.1161/STROKEAHA.114.007154.

Yang, W.-S., Li, Q., Li, R., Liu, Q.-J., Wang, X.-C., Zhao, L.-B., Xie, P., 2018. Defining the Optimal Midline Shift Threshold to Predict Poor Outcome in Patients with Supratentorial Spontaneous Intracerebral Hemorrhage. Neurocrit Care 28, 314–321. https://doi.org/10.1007/s12028-017-0483-7.

Zwanenburg, A., Leger, S., Vallières, M., Löck, S., 2020a. Image biomarker standardisation initiative. Radiology 295, 328–338. https://doi.org/10.1148/radiol.2020191145.

Zwanenburg, A., Vallières, M., Abdalah, M.A., Aerts, H.J.W.L., Andrearczyk, V., Apte, A., Ashrafinia, S., Bakas, S., Beukinga, R.J., Boellaard, R., Bogowicz, M., Boldrini, L., Buvat, I., Cook, G.J.R., Davatzikos, C., Depeursinge, A., Desseroit, M.-C., Dinapoli, N., Dinh, C.V., Echegaray, S., El Naqa, I., Fedorov, A.Y., Gatta, R., Gillies, R.J., Goh, V., Götz, M., Guckenberger, M., Ha, S.M., Hatt, M., Isensee, F., Lambin, P., Leger, S., Leijenaar, R.T.H., Lenkowicz, J., Lippert, F., Losnegård, A., Maier-Hein, K.H., Morin, O., Müller, H., Napel, S., Nioche, C., Orlhac, F., Pati, S., Pfaehler, E.A.G., Rahmim, A., Rao, A.U.K., Scherer, J., Siddique, M.M., Sijtsema, N. M., Socarras Fernandez, J., Spezi, E., Steenbakkers, R.J.H.M., Tanadini-Lang, S., Thorwarth, D., Troost, E.G.C., Upadhaya, T., Valentini, V., van Dijk, L.V., van Griethuysen, J., van Velden, F.H.P., Whybra, P., Richter, C., Löck, S., 2020b. The Image Biomarker Standardization Initiative: Standardized Quantitative Radiomics for High-Throughput Image-based Phenotyping. Radiology 295, 328–338. https://doi.org/10.1148/radiol.2020191145.